

Section 2

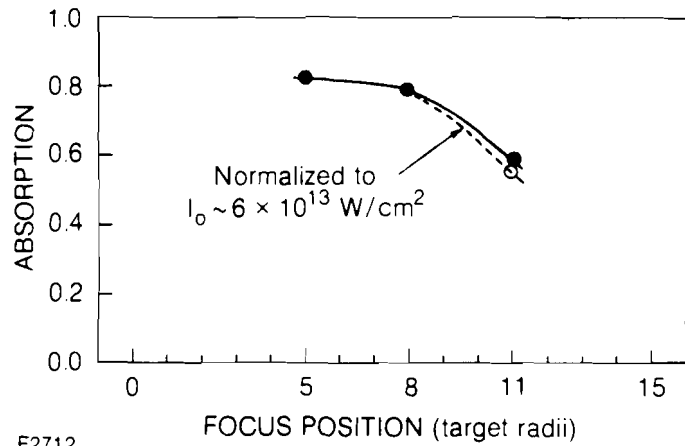
PROGRESS IN LASER FUSION

2.A Absorption and Hot-Electron Generation Measurements with Spherically Illuminated Targets at $\lambda=351$ nm

This section describes the measurements of laser-energy absorption and hot-electron production made on spherical targets irradiated with the six UV beams of OMEGA. These measurements have been conducted over a wide range of parameters. Incident energies in the range 160-298 J, with pulse durations of 600-700 ps, provided intensities across the range of 10^{13} - 2×10^{15} W/cm². The focus condition was varied between $F = -1R$ (surface-focus condition) through tangential focus ($F = 8R$) to well beyond tangential focus ($F = 11R$). Absorption was measured on solid spheres of various materials (CH, Al, Ti, and Ni), having diameters in the range of 80-1200 μ m. The principal diagnostic of absorption was an array of 20 differential plasma calorimeters located uniformly around the target. Additional data was also provided by two charge collectors positioned 75 cm and 175 cm from target and a 15-channel x-ray continuum spectrometer monitoring x-ray emission from 1-300 keV.

The absorption fraction as a function of the focus position of the beams is shown in Fig. 17.7. Measurements were made between $F = +5R$ and $F = +11R$ on 400- μ m-diameter CH spheres with incident energies of ~ 200 J. At nominal tangential focus ($F = +8R$) for the $f/3.6$ beams, the absorption is 80% at an incident intensity of 6×10^{13} W/cm². At $F = 5R$, beyond the limit for the minimum beam overlap on the target, the absorption is not significantly greater. However, at $F = 11R$ the laser beam overflows the target, and refractive losses are significant. Consequently, the absorption is markedly reduced ($\sim 60\%$).

Fig. 177
Absorption for 400- μm -diameter CH spheres for different focus parameters and for $\sim 200\text{-J}$, 650-ps pulses. The circle represents the result estimated for the same average on-target intensity at $F = +11R$ as at the other focal positions. This correction involves a normalization of the absorption efficiency according to measured intensity dependences.

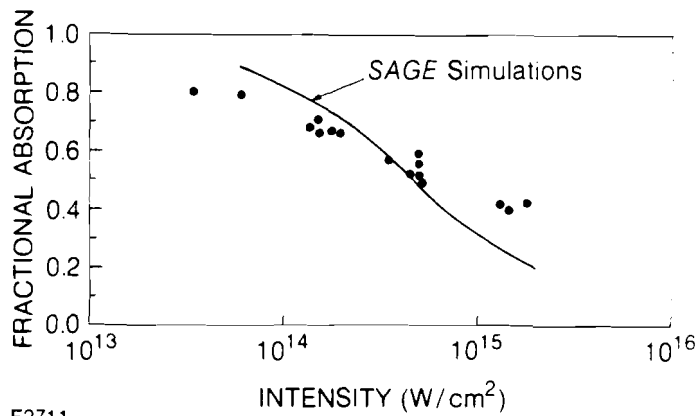


E2712

Correction of this net absorption value for the reduced average intensity resulting from the overflow and refraction losses, and, therefore, for the higher absorption efficiencies known to occur at lower intensities, decreases this value further. Thus, although higher uniformity is probably obtained with six beams focused beyond the tangential limit, this is only achieved at the expense of absorption. Consequently, all the parametric scaling of absorption was made for tangentially focused beams.

Figure 17.8 shows the variation of absorption with intensity for CH spheres varying in diameter between 100 μm and 420 μm for incident energies of the order of 200 J. It can be seen that the overall absorption drops from $\sim 80\%$ at low intensities to values of the order of 40% at intensities approaching 10^{15} W/cm^2 . Although subsequent data will establish that the principal absorption mechanism throughout

Fig. 17.8
Ultraviolet absorption for tangentially focused ($F = +8R$) $E_L = 160\text{-}298 \text{ J}$, $t_L = 600\text{-}650\text{-ps}$ pulses on targets with radii in the range 45-220 μm , all with $> 2\text{-}\mu\text{m}$ CH outer layers. The SAGE simulation curve is for 200-J, 600-ps pulses, assuming a flux-limit parameter $f=0.04$.

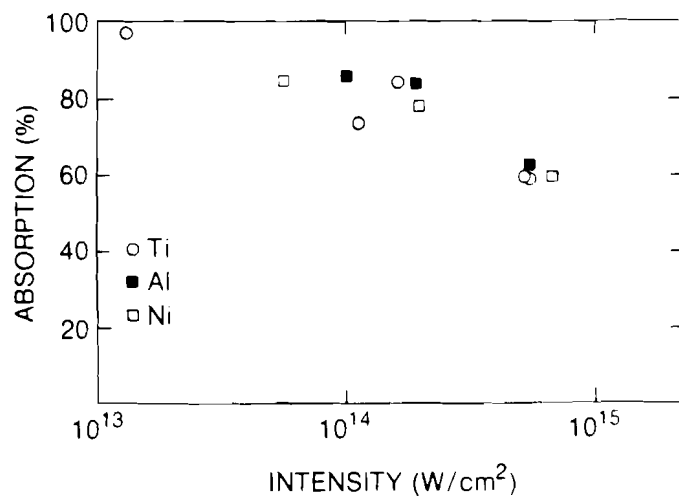


E2711

this range is inverse-bremsstrahlung absorption, the reduced absorption at high intensity is affected by the smaller target size (i.e., the small scale length). For the higher incident energies expected from full conversion of OMEGA to 351 nm, significantly higher absorption should be obtained at these intensities. Figure 17.8 also shows a comparison of the experimental data with one-dimensional SAGE calculations made assuming a flux-limiting parameter of $f = 0.04$. As can be seen, absorption significantly higher than predicted is obtained at high intensities, whereas at lower intensities the absorption is less than predicted. Although not plotted, a similar discrepancy exists between the experimental data and the predictions of the one-dimensional Lagrangian code, LILAC.

Figure 17.9 shows the absorption as a function of intensity for targets of various Z. Solid targets of aluminum, nickel, and titanium were shot at various intensities in the range 10^{13} – 10^{15} W/cm² with incident energies in the range 160–180 J. Measured absorption in excess of 95% was obtained at an intensity of 1.1×10^{13} W/cm². This measurement incidentally confirms the energy calibration between the plasma calorimeters and the optical calorimeters measuring output beam energy. The absorption on high-Z targets is somewhat greater than that on CH targets for comparable intensities, in agreement with previous measurements made on planar targets with GDL.¹

Measurements of hot-electron generation were obtained from x-ray continuum spectra from solid spherical targets irradiated with the six-beam ultraviolet OMEGA system. Estimates of the electron density and temperatures are found to show reasonable agreement with data obtained from the one-beam UV target experiments on GDL² and to support the argument that no significant preheat levels are evident in



E2828

Fig. 17.9
Absorption measurements using high-Z targets of various materials and radii (40–600 μm) with pulses ($E_L = 160$ –180 J, $t_L = 600$ –640 ps) at tangential focus ($F = +8R$).

spherical UV experiments, as compared to IR experiments. Incident energies in the range 160-200 J with pulse durations of 600-700 ps provided intensities across the range of $6 \times 10^{13} - 2 \times 10^{15}$ W/cm² at tangential focus (F=8R). The targets used were solid spheres having diameters of 80-420 μ m. The data to be shown here are from targets with a minimum of 4 μ m of CH over CH, Al, Ti, or Ni. To first order, hot-electron density and temperature scaling were obtained over similar ranges of intensity as the absorption measurements.

The principal diagnostic for measuring the level of hot-electron generation was a multichannel x-ray continuum spectrometer consisting of 9 PIN diodes and 6 PM-Nal scintillator detectors in conjunction with a wide variety of K-edge x-ray filters. The detector arrays incorporated lead collimators and shields to minimize pick-up of x rays from the target chamber walls. The PM detectors were calibrated using nuclear sources, and the sensitivity of the silicon diodes was obtained from known calibrations. The charge pulses from the detectors were integrated and recorded using gated analog-to-digital recorders. Additional oscilloscope monitoring was used to check for noisy or saturated signals. Table 17.1 shows the detectors and filters used. Since the individual detectors do not sample discrete energy bands in the x-ray spectrum, an interpolation approach to the estimation of the $dE/dh\nu$ curve is used. The approach taken in this work uses a multi-Maxwellian model to approximate the data. The spectrum is thus obtained globally rather than locally, the signals from individual detectors consequently contributing to broad regions of the spectrum. The points shown in the spectra correspond only to

Table 17.1.
OMEGA K-edge-filtered detector-system
parameters.

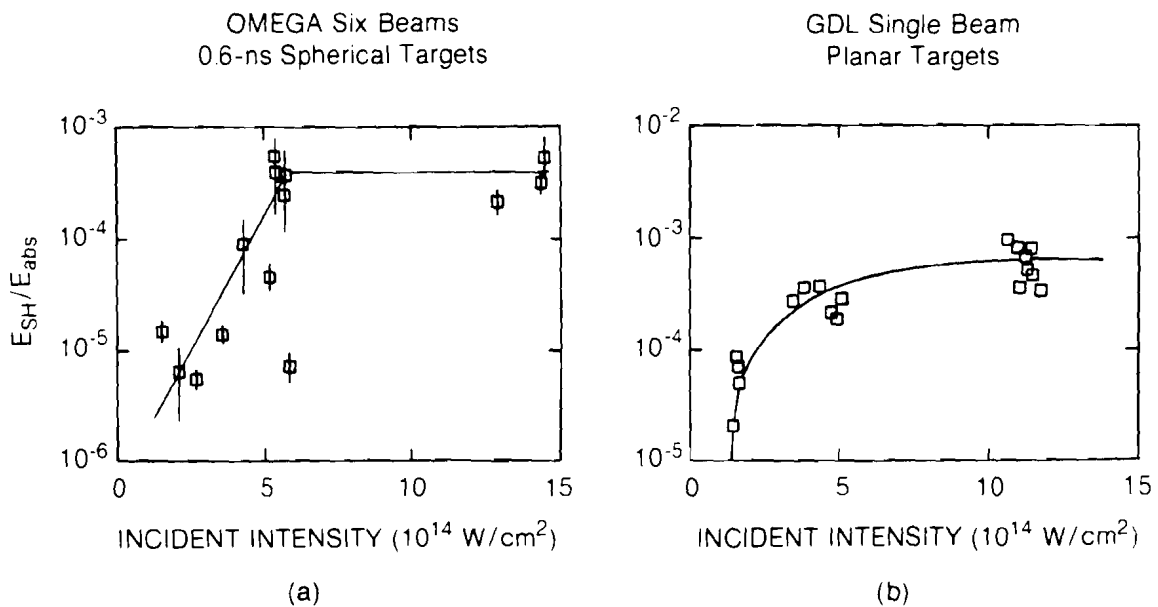
<u>Filter Material</u>	<u>Filter Thickness</u>	<u>K-Edge (keV)</u>	<u>Detector Material</u>	<u>Detector Thickness</u>	<u>Detector Type</u>
Cl (Saran)	50 μ m	2.8	Si	250 μ m	PIN
Sc	28	4.5	Si	250	PIN
Fe	25	7.1	Si	250	PIN
Ni	20	8.3	Si	250	PIN
Zn	47	9.7	Si	250	PIN
Y	253	17.0	Si	250	PIN
Mo	113	20.0	Si	250	PIN
Ag	136	25.5	Si	250	PIN
Ag	254	25.5	Nal	1 mm	PMT
Sn	250	29.2	Nal	1	PMT
Ta	507	67.4	Nal	1	PMT
Pb	1.0 mm	88.0	Nal	1	PMT
Pb	2.5	88.0	Nal	50	PMT
Pb	5.7	88.0	Nal	50	PMT

E2839

spectrum is observable [Figs. 17.10(a) and 17.10(b)]. Infrared irradiation of spherical targets at intensities of 10^{14} - 10^{15} W/cm² with nano-second pulses always resulted in the emission of a three-component spectrum comprised of a thermal electron component, a hot-electron component resulting from resonance absorption at critical density, and a superhot component resulting from hot-electron generation in the underdense corona. The two-component spectrum observed in all spherical UV experiments on OMEGA is clear evidence of the absence of resonance absorption in the interaction. This difference in the x-ray continuum spectrum between UV and IR irradiation in spherical geometry was previously observed in planar geometry on GDL.

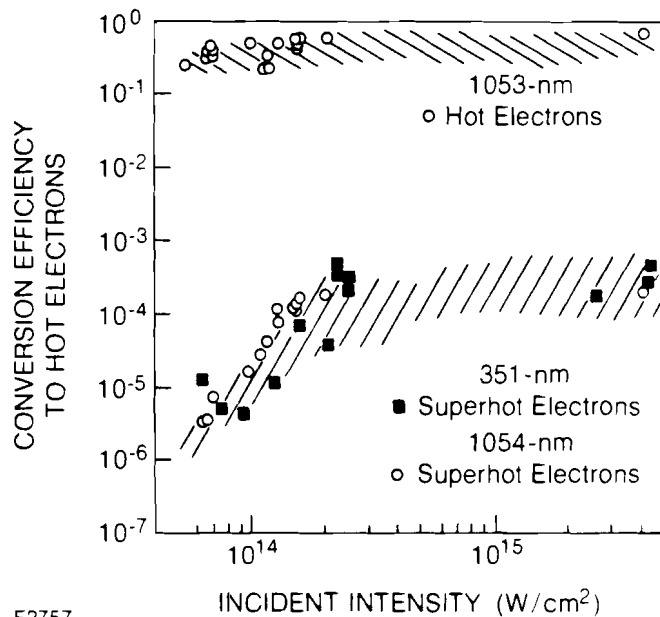
The relative partition of energy in the superhot-electron component for UV irradiation of spherical targets, as a function of intensity, is shown in Fig.17.11(a). This shows the ratio of the energy in the suprathermal tail of the distribution, normalized to the incident energy, as a function of incident irradiance, for CH targets of diameters ranging between 90 and 440 μ m. Although the data, particularly at lower intensities, shows considerable scatter, the general form of the intensity dependence is clear. At low intensities, the partition of energy to superhot electrons is extremely small and displays a sharp onset at an intensity $\sim 10^{14}$ W/cm². Moreover, at high intensities, there is clear indication under the prevailing conditions of a saturation in the conversion to superhot electrons at a level below 10^{-3} . Again, this data is remarkably similar to the earlier planar GDL results shown in Fig. 17.11(b).

Fig. 17.11
 Fraction of absorbed energy in the superhot-electron distribution with 351-nm illumination with (a) the six-beam OMEGA system and (b) the one-beam GDL system.



E2761

Plotted in Fig. 17.12 is the intensity dependence of the conversion efficiency to hot electrons (resulting from resonance absorption) measured in spherical IR experiments and the conversion efficiency to superhot electrons (from subcritical phenomena) measured in both IR and UV spherical experiments. Although the x-ray continuum spectrum overestimates the conversion of energy to hot electrons for IR experiments, the clear absence of resonance-absorption-generated hot electrons in UV spherical experiments clearly implies vastly reduced preheat levels for UV radiation.



E2757

Fig 17.12
 Fraction of absorbed energy in various hot-electron components at illumination wavelengths of 1053 nm and 351 nm. Because the hot component is absent at 351 nm, the total hot-electron preheat is substantially reduced at 351 nm.

Comparison of the level of hot-electron generation and the level of $3\omega_0/2$ harmonic emission provides some indication of the origin of the suprathermal electrons in UV-irradiated spherical plasmas. This comparison is shown in Fig. 17.13. As can be seen, there is a clear correspondence in the intensities at which both this harmonic and the generation of hot electrons commence in their similar intensity dependences. Moreover, saturation in the harmonic emission and in the suprathermal electron generation appears to occur at a similar intensity ($\sim 10^{15}$ W/cm²). Since there is strong evidence that the $3\omega_0/2$ harmonic emission originates from the $2\omega_p$ instability, this close correspondence in intensity dependence suggests strongly that the suprathermal electrons have a similar origin.

Summary

The measurements of the absorption, electron density, and temperature characteristics of UV-irradiated plasmas at high intensity show reasonable agreement with previous planar-target data and indicate significantly higher absorption and significantly lower preheat levels for UV irradiation, compared to IR experiments